Automatika

Journal for Control, Measurement, Electronics, Computing and Communications

ISSN: (Print) (Online) Journal homepage: www.tandfonline.com/journals/taut20

Detection of glioma on brain MRIs using adaptive segmentation and modified graph neural network based classification

V. Nagasumathy & B. Paulchamy

To cite this article: V. Nagasumathy & B. Paulchamy (2023) Detection of glioma on brain MRIs using adaptive segmentation and modified graph neural network based classification, Automatika, 64:4, 1268-1279, DOI: 10.1080/00051144.2023.2256521

To link to this article: https://doi.org/10.1080/00051144.2023.2256521

Published online: 20 Sep 2023.

AUTOMATIKA
2023, VOL. 64, NO. 4, 1268–1279
https://doi.org/10.1080/00051144.2023.2256521

Detection of glioma on brain MRIs using adaptive segmentation and modified graph neural network based classification

V. Nagasumathy[a] and B. Paulchamy[b]

[a]Department of ICE, Government Polytechnic College for Women, Madurai, India; [b]Electronics and communication Engineering, Hindustan Institute of Technology, Coimbatore, India

ABSTRACT

Gliomas constitute the prevalently seen brain tumours in humans. The real-time utilization of Computer Aided Diagnosis system depends on brain Magnetic Resonance Imaging (MRIs) has the ability of helping radiologists and professionals to identify the presence of glioma tumours. It is very difficult to segment brain tumours because of the brain image and it has a complex structure. A fully automated, accurate, segmentation and classification model is developed using a modified Graph Neural Network (MGNN) for brain tumours. Proposed work steps are, image registration, Shift-Invariant Shear let Transform (SIST), adaptive segmentation, feature extraction, and categorization of tumours. At first, image registration and SIST are carried out to improve image quality. Adaptive segmentation is then carried out utilizing Improved Fuzzy C-Means clustering. Next, Grey Level Co-occurrence Matrix, Discrete Wavelet Transform is utilized for the extraction of features in brain MRI data. Finally, MGNN is introduced for the detection of anomalous tumour-infected MR and actual MR brain images. The findings are demonstrated that the proposed model leads in higher accuracy levels for both classification and segmentation.

ARTICLE HISTORY
Received 30 May 2023
Accepted 1 September 2023

KEYWORDS
Gliomas; image registration; shift-invariant shear let transform (SIST); improved fuzzy c-means (IFCM) clustering; grey level co-occurrence matrix (GLCM) and discrete wavelet transform (DWT); modified graph neural network (MGNN)

1. Introduction

Glioma is the most prevalent kind of primary brain tumour. They start in the brain's glial cells and are often classified into many classes, including: While Low-Grade Gliomas (LGG) are slow-growing tumours with a better prognosis for patients, High-Grade Gliomas (HGG) develop swiftly and are extremely malignant [1]. Assessment of the disease's course, planning of treatments, and evaluation of brain tumours all depend on MRI.T1-weighted, T2-weighted, contrast-enhanced T1-weighted (T1ce), and Fluid Attenuation Inversion Recovery (FLAIR) images are some of the MRI sequences that may be used to scan brain tumours [2]. In contrast to T1 and T1ce pictures, which provide better contrast for the tumour core area, T2 and FLAIR images mainly concentrate on the whole tumour region. Hence, these various sequences yield additional information can be integrated for analysing various sub regions of brain tumours. One of the most dangerous brain conditions, brain tumours may arise because of abnormal cell growth inside the skull [3]. Primary and secondary brain tumours are the two categories into which they may be divided. In contrast to secondary brain tumours, which initially form in the breast, kidney, or lung before moving to the brain, for 70% of all tumour forms, primary brain tumours are the only ones that are seen. According to a study by the NBTF, there are about 29,000 primary brain tumour diagnoses in the US alone each year, and 13,000 of those instances result in fatalities. Similar to this, every year in the UK, over 42,000 individuals must deal with the mortality due to primary brain tumours. Gliomas, meningioma's, and pituitary tumours are the three most common forms of brain tumours [4]. Glial cells, which make about 80% of the brain, may grow into glioma tumours.

Its death rate is one of the highest of all primary malignancies. Tumours called meningioma's develop inside the meninges, the brain's protective covering. As opposed to this, the pituitary gland's tumour develops there. This gland generates different hormones that are required [5]. Due to the benign nature of the pituitary tumour, hormonal deficiencies and irreversible danger to vision can occur. Therefore, it is required to have a proactive and exact diagnosis of brain tumours to safeguard the patients from dangerous conditions. MRI is one of the techniques for the routine identification of different types of tumours, and each kind of tumour manifests itself on the MRI picture with a unique contrast. The MRI will help the doctor diagnose the tumour more accurately so that they can prescribe a course of therapy that is appropriate for the patient's condition, taking into account cancer's location, size, shape, kind, and level. However, since these characteristics vary from patient to patient, accurate categorization and improved cancer diagnosis are required to provide access to better therapy. Additionally, a manual

CONTACT V. Nagasumathy v.nagasumathi@gmail.com Department of ICE, Government Polytechnic College for Women, Madurai, India

approach for tracking a tumour's progress and visual identification by a clinician is usually prone to mistakes, necessitating the development of an automated system to recognize and categorize tumours. Important stages in the categorization of brain tumours include removing the form and texture of the areas of interest from the MRI picture. Any CAD system's strength is dependent on two key components: one related to the stages of pre-treatment and tumour detection, and the other to tumour categorization [6].

Automatic segmentation of brain tumours and sub regions using multimodal MRI is crucial to provide a consistent and reliable measurement of the tumours and to assist in diagnosis, treatment planning, and improvement assessment [7]. But using automated methods to reliably distinguish brain tumours from multi-modal MRI is difficult. This is because the borders between the healthy tissues and brain tumours are typically blurry in the photographs. Even while the information regarding shape and position has been utilized to separate anatomical systems like the liver and the heart, the shape, size, and location of brain tumours vary greatly across different people. Because of this, it is difficult to reliably separate brain tumours using an existing form and location [8]. Machine learning (ML)-based techniques and deep learning (DL)-based methods may be used to classify brain tumours, respectively. Prior to classification, Manual feature extraction and segmentation, which takes a lot of time and is prone to error, are performed by ML-based systems [9]. To accomplish tumour detection in a more effective way, these methods often need the assistance of a qualified expert who is familiar with discovering the optimum feature extraction and segmentation algorithms. The speed obtained with these methods is thus subject to errors when working with larger datasets. At the same time, these processes are carried out automatically using DL-based algorithms, which are shown to be very beneficial in a variety of applications, such as medical picture analysis. Due to its dependable performance and weight-sharing feature, the graph neural network (GNN), one of the popular DL models, is widely employed. From training data, it can automatically extract both low-level and high-level characteristics. Brain tumour segmentation is a huge challenge since brain image and its structure are complex, whose analysis can be done performed through expert doctors or radiologist. This study presents an automated approach for reliably classifying and segmenting brain tumours that makes use of an MGNN.

1.1. Major contribution of the work

The real-time utilization of CAD system depends on brain MRIs has the ability of helping the radiologists and professionals to identify the presence of glioma tumours. To segment brain tumours, a fully automated, accurate, segmentation and classification model is developed using a MGNN for brain tumours.

The remainder of the research project is divided into the following sections: The current methods for identifying brain tumours are summarized in section 2. Section 3 describes the general procedure used in the suggested method. Section 4 presents the results and analysis. Section 5 discusses the results and the next tasks.

2. Literature review

This section provides an outline on few current approaches used for the brain tumour detection applying supervised and unsupervised machine learning algorithms.

Selva pandian et al. [10] presented in order to enhance the brain picture, a Non-Sub sampled Contour let Transform (NSCT) is used, and from the improved brain image, texture characteristics are then extracted. The Adaptive Neuro Fuzzy Inference System (ANFIS) approach is used to train these characteristics and categorize them into the normal and glioma brain images. Later, morphological functions are used to produce the segmentation of the tumour areas in the glioma brain picture. On the Brain Tumor Image Segmentation Challenge (BRATS) open access database, the suggested Glioma brain tumour identification method is used for performance assessment.

Mathiyalagan et al. [11] designed a machine lear ning-based classification method using brain magnetic resonance imaging (MRI) that is computer-aided and completely automated to identify and classify gliomas. After the noise has been removed from the picture, fuzzy logic is used to locate the image's edges. The noise contents in the source brain MRI image are first identified and removed with the aid of ridge let filter. On the image of the augmented brain, the Gabor transformation is performed, and the resulting changed image is what is utilized for calculating the features. The source brain MRI image is classified as either having glioma or not having glioma using the ANFIS classification technique. The optimized features are then classified using the feature optimization approach genetic algorithm (GA), which performs the optimization of the computed features. The glioma brain image is eventually employed using fuzzy C methods to divide the tumour spots. Segmented tumour locations in glioma brain pictures are compared to manually segmented tumour areas to assess how well the suggested approach works. The simulation findings show that the recommended works in this survey perform at the highest level when compared to benchmark methodologies. Kibriya et al. [12] studied about novel deep feature fusion-based multiclass brain tumour classification method. Min–max normalization is utilized to preprocess MR pictures, and extensive data augmentation

is then performed to address the issue of data deficiency on MR images. The deep CNN features obtained from transfer learning architectures like AlexNet, Google Net, and ResNet18 are combined to generate a single feature vector that can be fed into support vector machines (SVM) and K-nearest neighbour (KNN) for the prediction of the final output. Given that the new feature vector includes a lot more information than the individual vectors do, the recommended strategy performs better in terms of classification. The suggested model is trained on 15,320 MRIs and its performance is evaluated. The research shows that, in comparison to independent vectors, the feature vector performs much better. It may be used in clinical settings for classifying brain cancers from MRIs since it performs much better than the existing methods and produces an accuracy of 99.7%.

Demir et al. [13] presented an innovative and efficient technique that depends for identifying brain tumours from MR image samples using a deep auto encoder. Convolutional layers, rather than dense layers, were used in the deep auto encoder design. The deep auto encoder model's last encoded layer was used to extract the deep feature sets. The variance threshold technique reduced the depth of the features. The classification procedure used a variety of classifiers, including SVM, DT, KNN, and ensembles. The SVM classifier was used in conjunction with the RBF kernel to get the best classification metrics. The performance of the proposed method is compared to that of the current methods using the same database and deep learning models like VGG16 and Alex Net models.

El Hamdaoui et al. [14] introduced a smart clinical decision support system to detect and classify Risk of Malignancy Index (RMI) images of brain tumour. In order to get over the problem of labelled training data deficit, it is necessary that convolutional neural networks need to be trained, and therefore it is essential to study transfer ideas deeply and stack them. Instead, the brain tumour segmentation (BraTS) 19 database is used. This database is comprised of seven CNN frameworks that have been pre-trained on an Image Net database. This ImageNet database is designed to be an exact fit on magnetic resonance imaging (MRI) of brain tumours. To improve the precision of the universal model, the prediction from among the seven pre-trained CNNs that scored best is utilized as the prediction. A 10-way cross-validation approach is used to evaluate the performance of the primary 2-class model for LGG and HGG brain tumours. With mean test precision of 98.67%, mean f1 score of 98.62%, test precision average of 98.06%, and average test sensitivity of 98.33%, the recommended model is much more efficient than others that have been published. The suggested model's results are contrasted with those that have been documented in the literature.

Naser et al. [15] recommended a deep learning mechanism, based on a pre-trained convolution-base of Vgg16 and a fully connected classifier for tumour grading, which includes CNN that relies on the U-net for tumour segmentation and transfer learning. The same pipeline of T1-precontrast, FLAIR, and T1-postcontrast MRI images from 110 LGG patients is used by the segmentation and grading algorithms for training and evaluation. With the assistance of the segmentation model, the average dice similarity coefficient (DSC) and tumour identification accuracy were found to be 0.84 and 0.92, respectively. With an accuracy, sensitivity, and specificity of 0.89, 0.87, and 0.92, respectively, at the level of the MRI images and 0.95, 0.97, and 0.98, respectively, at the level of the patients, the grading model divides LGG into grades II and III.

Alnowami et al. [16] presented an automatic technique for the MRI scans can identify brain tumours. In order to do so, this study took into account around 4314 MRI pictures. Four types of data are present: photos of the pituitary tumour, glioma, and meningioma in addition to photographs of a healthy brain. The accuracy of the model was evaluated after each preprocessing step that the raw data went through. Three different datasets were used to train a densely connected convolutional network (Dense Net). The classification accuracy is increased by enhancing the contrast and normalizing the intensities of the MRI picture. The learning convergence of Denseness training is shown to be increased by the pre-processing stages. Applying ten-fold cross-validation, the suggested model achieves a 96.52% accuracy rate, 98.5% sensitivity, and 82.1% specificity, respectively.

Using the available models, through the inclusion of domain-based existing knowledge, they assist in directly modelling the probability distributions of anatomical features and the textural appearances of healthy tissues and the tumour, generative approaches often exhibit high generalization to unknown pictures. It is difficult to describe the probabilistic distributions of brain tumours precisely, nevertheless. Discriminative approaches, on the other hand, undertake feature segmentation and extraction from pictures, and then use discriminative classifiers to correlate the features with tissue types. Therefore, this work highlights on the reliable segmentation and effective classification approaches for the exact results. Table 1 shows comparative analysis of the existing approaches.

3. Proposed methodology

This study presents an automated approach for reliably classifying and segmenting brain tumours that makes use of an MGNN. Image registration, SIST, adaptive segmentation, feature extraction, and tumour classification are the five processes in this suggested module. SIST and image registration are initially used to

Table 1. Comparative analysis of the existing approaches.

Author name	Approaches	Strengths
Selvapandian et al. [10]	Non-Sub sampled Contour let Transform (NSCT)	Glioma brain tumour identification
Mathiyalagan et al. [11]	Adaptive neuro fuzzy inference system (ANFIS)	Automated to identify and classify gliomas
Kibriya et al. [12]	Support vector machines (SVM) and K-nearest neighbour (KNN)	Brain tumour classification, achieved higher accuracy
Demir et al. [13]	support vector machines (SVM)	Accurate identifying brain tumours
El Hamdaoui et al. [14]	Convolutional Neural Network (CNN)	LGG and HGG brain tumours
Naser et al. [15]	Convolutional Neural Network (CNN)	Improved average dice similarity coefficient (DSC) and tumour identification accuracy
Alnowami et al. [16]	Densely connected convolutional network (DenseNet)	Classification accuracy is increased

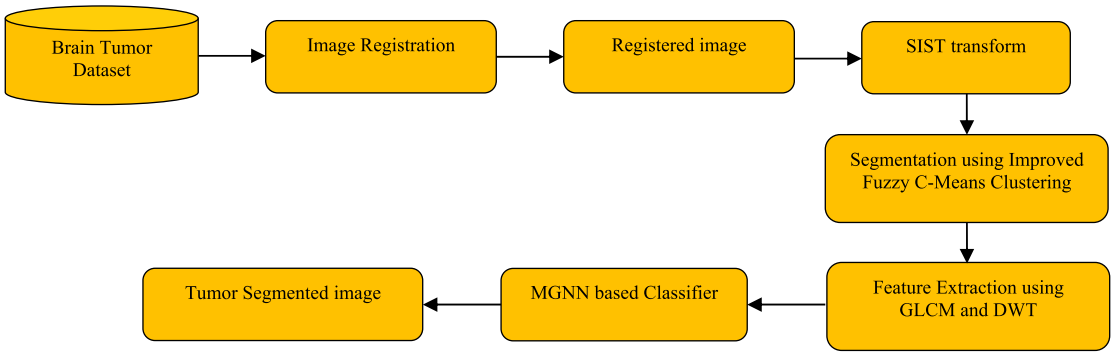

Figure 1. Process of the proposed brain tumour segmentation.

enhance the picture quality. In order to get superior segmentation results, adaptive segmentation is then carried out with the aid of IFCM clustering. Then, to extract features from the brain MRI data, the GLCM and DWT are used. In order to distinguish between MR brain pictures with abnormal tumour infection and those with normal tumour infection, the MGNN is finally introduced. The suggested approach's workflow is shown in Figure 1.

3.1. Image registration

The test brain data are aligned with the reference brain picture using a linear registration method in this study. The picture registration is shown below method as,

Step 1 : Create 3*3, non-interfering sub blocks from the source and reference brain images.

Step 2 : Use the following calculation to calculate these two distinct, non-overlapping sub blocks' cross correlation:

$$NCC = \frac{1}{N}\sum_{\vec{X}_{\in br}} \frac{\left|b_r\left(\bar{\bar{x}}\right) - \mu x^*\right| b_r || b_f\left(\bar{\bar{x}}\right) - \mu y^*) b_f}{\sigma s^* b_r \times \sigma r^* b_f} \quad (1)$$

where N indicates how many pixels there are overall in the 3∗3 sunblock"σs" and "σr" the source and reference sub blocks' respective standard deviations "μx" and "μy" refer to the average of the source sub blocks as well as the reference sub blocks.

Step 3 : If the estimated cross correlation is less than the threshold value, the pixels in the reference image are warped in the direction of their corresponding pixels in the source brain image. The threshold is computed by averaging the means of the source and reference sub block pixels.

Step 4 : Next, each sunblock in the source and reference brain images is subjected to the same procedure.

3.2. SIST transform

The SIST, which has two stages: multi- and spatial localization, is used in this study to merge the two brain scans to enhance the image of the brain. The Gibbs effect is significantly decreased when a non-sample pyramid filter scheme is used by swapping out the down-samples $f(i,j)$, as indicated in the equation below. It is possible to demonstrate that the shift invariance is less sensitive to image shift in a multiscale partition as a consequence.

$$f'_k(i,j) = f(i,j)^* h_k, \quad (2)$$

where h_k indicates the pyramid filter's central component. The resulting frequency plane is split into low-frequency sub bands and several high-frequency trapezoidal sub-bands in accordance with the directed localization principle using shift-invariant shear filters. The image sources Due to the uneven visibility in the cells in both the intensity (I) of the source picture and the sub bands SHI of the MR brain transformation, before the SIST convert. These I sub bands are transformed by the SIST into sub bands with high- and low-pass properties.

Using the arithmetic fusion approach, the coefficients of the output sub bands are combined.

3.3. Adaptive segmentation using improved fuzzy c-means (IFCM) clustering

One of the widely used techniques for picture segmentation is known as the fuzzy c-mean algorithm. This algorithm works by dividing the image space into several clusters, each of which contains pixels whose values are similar to those of the others [17]. It is a clustering approach that makes it possible for each cluster to include data items with varying degrees of belonging. By lowering the weighted within group sum of squared error goal function, the technique, which employs an iterative clustering strategy, produces an ideal c partition.

Let $X = \{x_1, \ldots\ldots, x_n\}$, let c represent a positive integer greater than one in a database. Mutually disjoint sets provide the c-cluster division of $X, X_1, \ldots., X_c$ such that $X_1 \cup \ldots.. \cup X_c = X$ or utilizing the indication function in a similar manner $\mu_1, \ldots\ldots \mu_c$ so that $\mu_i(x) = 1$ if x is in X_i and $\mu_i(x) = 0$ if x is not in X_i for all $i = 1, \ldots\ldots, c$. Clustering X into c clusters is what this is known as $X_1 \ldots..X_c$ using $\{\mu_1, \ldots\ldots \mu_c\}$. A fuzzy extension permits $\mu_i(x)$ using the values in the range [0, 1] such that $\sum_{i=1}^{c} \mu_i(x) = 1$ for all x in X. Here, $\{\mu_1, \ldots\ldots \mu_c\}$ is known as a fuzzy c-partition of X. Therefore, the FCM objective function J_{FCM} is specified as

$$J_{FCM}(\mu, v) = \sum_{i=1}^{c} \sum_{j=1}^{n} \mu_{ij}^{m} d^2(x_j, v_i), \tag{3}$$

where $\mu = \{\mu_1, \ldots\ldots \mu_c\}a$ c-partition that is fuzzy and has $\mu_{ij} = \mu_i(x_j)$, A fixed value greater than one that indicates the level of fuzziness is used to determine the weighted exponent, or m, $v = \{v_1, \ldots\ldots v_c\}$ represents the centres of the c cluster, and $d^2(x_j, v_i) = x_j - {v_i}^2$ indicates with its generalization, the Euclidean distance. Utilizing the following update equations, the FCM method simply iterates over the circumstances necessary to minimize the J_{FCM}:

$$v_i = \frac{\sum_{j=1}^{n} \mu_{ij}^{m} x_j}{\sum_{j=1}^{n} \mu_{ij}^{m}} (i = 1, \ldots\ldots c) \tag{4}$$

and

$$\mu_{ij} = \frac{1}{\sum_{k=1}^{c} \left(\frac{d(x_j, v_i)}{d(x_j, v_i)} \right)^{2(m-1)}} \tag{5}$$

During every iteration, μ and v get revised applying (4) and (5). The FCM algorithm performs the iterative optimization of $JFCM(\mu, v)$ until $|\mu(l+1) - \mu^l| \leq \varepsilon$ refers to the number of iterations.

It is clear from (3) that every picture pixel is regarded as an independent point and that the objective function of FCM does not take spatial interdependence among X into account. In addition to this, the function for determining membership in (5) is chosen by $d^2(x_j, v_i)$, it calculates the degree to which the cluster centre's centre and the pixel intensity are comparable. The value of membership increases with the degree of closeness the intensity values show to the cluster centre. As a result, noise greatly affects the membership function. In the event that noise or other artefacts impair a picture, there would be a change in intensity of the pixels that leads to imprecise membership and uneven segmentation.

3.3.1. Adaptive distribution factor

In order to get over these disadvantages, in this research, an enhanced algorithm is presented. In this technique, a type of correlation referred as Adaptive Distribution factor is found to be present involving neighbourhood pixels. Every pixel seeks to attract pixels in its neighbourhood to its own cluster while clustering is taking place. The pixel intensities or feature attraction are two factors that this adaptive distribution factor depends on $\lambda(0 < \lambda < 1)$, given the neighbours' physical locations or the appeal of distance $\xi(0 < \xi < 1)$, this is dependent on the neighbourhood's shape as well. The provided value for this adaptive distribution factor is

$$d^2(x_j, v_i) = x_j - {v_i}^2 (1 - \lambda H_{ij} - \xi F_{ij}) \tag{6}$$

where H_{ij} stands for the main attractions and F_{ij} indicates the distance attraction. The parameters λ and ξ modify the size of the two neighbouring attractions. H_{ij} and F_{ij} are calculated in neighbourhood having S pixels in the equations:

$$H_{ij} = \frac{\sum_{k=1}^{S} \mu_{ik} g_{ik}}{\sum_{k=1}^{S} g_{ik}} \tag{7}$$

$$F_{ij} = \frac{\sum_{k=1}^{S} \mu_{ik}^2 q_{jk}^2}{\sum_{k=1}^{S} g_{jk}^2} \tag{8}$$

with

$$g_{jk} = |x_j - x_k|, q_{jk} = (a_j - a_k)^2 + (b_j - b_k)^2 \tag{9}$$

where (a_j, b_j) and $(a_k - b_k)$ indicating, respectively, the coordinates of the pixels j and k. It is necessary to keep in mind that a greater value of λ results in a very attractive feature that is extremely coherent, and the value of ξ produces a highly cohesive attraction at a distance. These parameters' ideal values provide wonderful segmentation outcomes.

3.4. Feature extraction

In this study, tumour areas identified in brain MRI data were diagnosed using the features of GLCM and DWT. For the purpose of locating and diagnosing brain tumours, a characteristic is used to identify differences between normal patterns and aberrant patterns.

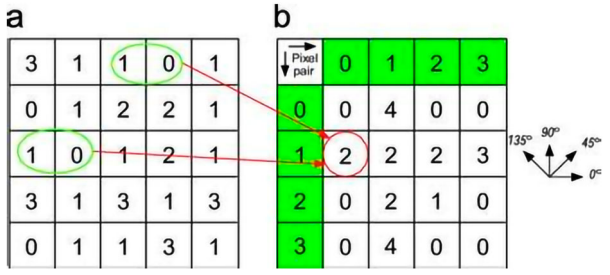

Figure 2. Generation of GLCM feature extraction.

3.4.1. GLCM features

The generation of GLCM feature extraction shown in Figure 2. The pre-processed MRI brain image's GLCM characteristics help to achieve the correlation between the different pixels. In a the Figure 2 picture that has been pre-processed and has many orientations, including 0, 45, 90, and 135 degrees, the GLCM data matrix represents the frequency of repetition of pixels. The following GLCM characteristics are used in this technical effort to produce contrast, homogeneity, and energy correlation in the GLCM matrix.

$$Contrast = \sum (|a-b|^2 \times p(a,b)) \tag{10}$$

$$Energy = \sum p(a,b)^2 \tag{11}$$

$$Homogeneity = \frac{\sum p(a,b)^2}{1+|a-b|} \tag{12}$$

$$Correlation = \sum (a-\mu a)(b-\mu b)\frac{p(a,b)}{[\sigma a, \sigma b]} \tag{13}$$

The a, b are parameters of the homogeneity.

3.4.2. Wavelet features

In this study, brain data are classified into normal and pathological types using wavelet characteristics derived from the changed brain picture. The NSCT transform's coefficients are used to perform the 2D-Discrete Wavelet Transform (DWT). Vertical, Approximate, Diagonal, and Horizontal sub bands are created by dividing the changed image into these four groups.

3.5. Modified graph neural network based classification

Presently, Graph Neural Network (GNN) has emerged immensely popular in different fields. The strength of GNN with regard to the modelling of the dependencies between nodes in a graph facilitates the big leap made in the research domain associated with graph analysis. GNN [18] is a specific kind of Neural Network that operates on the Graph format straight away. A common application of GNN involves node classification. The objective is to estimate each node's label without needing any ground truth since each node in the graph has a label.

Figure 3 shows the workflow of the proposed model for predicting the disease. Next, through the measurement of the closeness of any illness to the patient's embedding, gradually the probability of patient p diagnosis with disease is estimated. In order to create a low-dimensional embedding, a graph encoder model is described in this section's first paragraph z ∈ Rd for every node in an arbitrary graph. Taking inspiration from the current progress in graph convolutional networks, using an aggregation method, each node's embedding is calculated based on the characteristics of its immediately connected neighbours. The first-order neighbours of a node are taken into account by the supplied aggregation function, and the same modification is applied to all the nodes in the network. Every node in the network provides its own input field for calculation in this fashion, but throughout the computations of different nodes, the same parameters specifying how information is exchanged and dispersed are reused. With this design, the graph's information that is scattered across regions is used efficiently, and it is possible to create embedding during training for previously unknown nodes, such as a newly joined patient in the database.

To start with, for a graph $G = \{C, P\}$, showing a disease, symptom, or patient node in a consistent manner be$v \in G$ that is compact. Later, at the l-th layer of information transmission, the embedding $\mathbf{h}lv$ of node v is computed as:

$$h^l_{N_{(v)}} = AGGREGATE(\{h^{l-1}_{v'}, \forall v' \in N(v)\}) \tag{14}$$

$$h^l_v = \sigma(W^l.[h^{l-1}_v; h^l_{N(v)}]) \tag{15}$$

where W^l refer to the weight matrix, whose learning is to be done at the l-th layer, h^{l-1}_v stands for the node v's embedded at a prior layer, and the total layer size is represented as L. [.;.] indicates concatenating two vectors, and $N(v)$ is used for specifying the set of uniformly sampled neighbour nodes of v. it is to be observed that for $l = 0$, the initialization of the node embeddingh0v∈Rd either random numbers or side information from the data are used to do this. For instance, utilizing a patient node and the patient demographics and medical profiles already included in the EMR data, h0v will be turned into a real-valued dense feature vector with every digit reflecting the observed value of a feature dimension (e.g. age). h$lN(v)$ represents the synergic representation that is produced as a consequence of the aggregation function, which was devised for the purpose of aggregating the embedding of node v's. Neighbours at the (l-1)-th layer. Σ is an activation function that is not linear (e.g. tanh), as well as choosing between mean, maximum pooling, RNNs, etc. as the aggregator. The default, *mean* (′) aggregates information using in the model. Before obtaining the final embedding for each node at the final layer L,

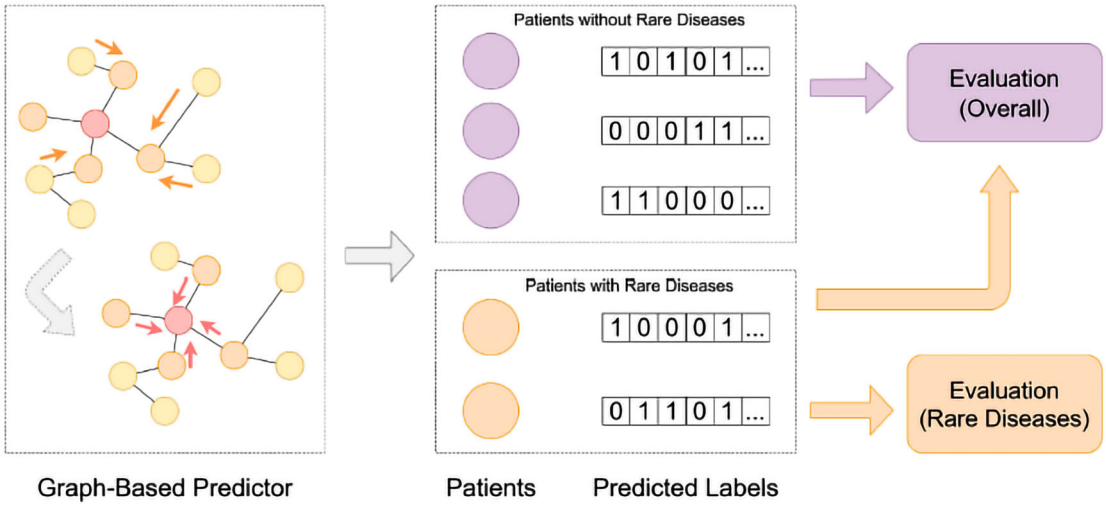

Figure 3. The method used by the illness prediction model based on graph neural networks.

a normalizing step is needed later:

$$h_v = \frac{h_v^L}{h_{v2}^L}, \forall_v \in g \tag{16}$$

In this research, it has to be observed that the representations whose learning is done using the embedding space of the symptom nodes in the patient record graph P and the medical concept graph C are identical. In other words, every symptom's embedding in both graphs is the same for every symptom p, serving as a useful filler in many networks between patient and sickness nodes. Projecting every node embedding into the same space further aligns their contexts prior to a non-linear activation. Three separate embedding spaces are used to execute the learning of the illnesses, patients, and symptoms in this process, which is done concurrently in the form of various sorts of nodes:

$$z_v = \sigma(Wh_v), \forall_v \in g \tag{17}$$

where zv denotes the final embedding for node v and W denotes the learnable projection weight. But, it is not capable of processing the edge information (e.g. various edges in a knowledge graph may specify diverse associations between nodes). In addition, a static point cannot promote the diversity of node propagation, and therefore may not be desirable for learning during the node representation. Therefore, in this technical work, a Patrice Swarm optimization algorithm is presented with the aim of finding a solution to the above stated issue.

- **Particle Swarm Optimization (PSO)**

To find the best answer, a swarm that roams the search region is one of the particles used by PSO [19]. Every particle may be seen as a point in a D-dimensional space, and each point changes how it is "flying" based on both its own flight history and the flying histories of the other particles that are still around. The particles in the D-dimensional space must travel at a certain speed for the optimal outcome.

The definition of the particle's I velocity is $V_i = (v_{i1}, v_{i2}, \ldots, v_{iD})$, the particle's position is shown by $(x, x_{i2}, \ldots, x_{iD})$, the best place for particle I to be was given as $p_g = (p_{g1}, p_{g2}, \ldots, p_{gD})$, another name for it is p_{best}.

All particles are at their maximum possible position globally when $p_g = (p_{g1}, p_{g2}, \ldots, p_{gD})$, another name for it is g_{best}. Each particle in the group has a fitness function to determine the fitness value. The velocity update equation for the dimension d is provided by formulae (18) and (19) in traditional PSO:

$$v_{id} = w \times v_{id} + c_1 \times rand() \times (p_{id} - x_{id}) + c_2 \times Rand() \times (p_{gd} - x_{id}) \tag{18}$$

$$(X_{id} = x_{id} + v_{id}) \tag{19}$$

PSO parameters are: The terms "Q" stands for "Population Quantity", "w" for "inertia weight", "C1 and C2 for acceleration constants", "$v_{\max}$" for "maximum velocity", "$G_{\max}$" for "highest number of iterations", and "rand" and "Rand" for "random functions" with values between [0,1]. Constant 2 is generally used to calculate C1 and C2 values.

To overcome the limitations of standard optimization algorithms and address multi parameter, tight coupling, and nonlinear engineering optimization concerns, the EPSO enhances information transmission across populations and maintains population diversity throughout the optimization process. These negatives include enhanced convergence and a propensity to quickly enter local optimization. After evaluating the parameters used in the imported data, the idea of parameter selection for performance is decided "local-global information sharing" phrase. The EPSO and traditional optimization techniques both produced effective results, as seen in later validated with several sets of

conventional functions with the intent of verifying the global search performance of the EPSO.

The objective of this research is to present a EPSO form, which attempts improving the performance achieved with the PSO algorithm in getting superior solutions when maintaining both its simplicity and its rapid convergence [20]. This collision factor depends on presenting an ordinary but efficient novel operation in the iterative search process for improving the strength of the algorithm in both the exploration of new fields of the search space containing optimal solutions and exploitation of intermediate solutions. The modified PSO variation that relies on parameter settings is where the suggested version starts.

- **Collision factor**

Since the dimensions corresponding to a text feature vector in text classification are often fairly large, the particles in PSO will build up to a point where it is still impossible to get the global optimum. To ensure that the best convergence is obtained, the collision factor K is added to PSO. Formula (20) gives the velocity expression:

$$v_{id} = K[v_{id} + c_1 \times rand() \times (p_{id} - x_{id}) + c_2 \times Rand() \times (p_{gd} - x_{id})] \quad (20)$$

Algorithm 5.1 in this work utilizes the expression above to compute the collision factor K. When Clerc's experiment was employed, values c1 and c2 were both reached using a value of 2.05, which was the same. K is designated for experimentation with four decimal places here. The specific velocity expression is provided by formula (5.3) as follows:

$$v_{id} = 0.7298 \times [v_{id} + 2.05 \times rand() \times (p_{id} - x_{id}) + 2.05 \times Rand() \times (p_{gd} - x_{id}) \quad (21)$$

For the first iterations, to identify the likely placement of the ideal solution, a particle in PSO must conduct detection across a significant time period. To determine the perfect point in the next repetitions, it must expand locally for a brief period of time. K must thus utilize a larger number early on and a smaller one afterwards. K must also steadily decrease over a lengthy period of time in the latter phase, reaching its minimum. This variation pattern demonstrates congruence with the concave function.

The first iterations of the collision factor must choose a convex function so that the particles may reach the optimal solution over a long period of time in order to avoid early convergence. In the advanced iterations, a concave function has to be chosen so that the collision factor can vary gradually to the minimum for the local development. Convergence of the algorithm is guaranteed here. As per this concept, the functional collision factor that are formed based on the cosine function is given in expression (22):

$$K = \frac{\cos((\pi / G_{max}) \times T) + 2.5}{4} \quad (22)$$

T is the number of iterations in this sentence. Initialize $G_{\max} = 40$, in perspective of the value K's changing curve. Initially having a convex function, the K curve eventually becomes concave. The value K is replaced in formula (22), and later formula (22) changes into formula (23). Formula (23) is given as follows:

$$v_{id} = \left(\frac{\cos((\pi \times T/G_{max})) \times 2.5}{4}\right) \times [v_{id} + 2 \times rand() \times (p_{id} - x_{id}) + 2 \times Rand() \times (p_{gd} - x_{id})] \quad (23)$$

4. Results and discussion

In this study, the suggested MGNN classification algorithm for brain tumour detection pictures is tested using MRI data that was obtained via the brain tumour dataset (kaggle). The 3.1 GHz GPU processor and 4 GB of internal RAM are used to implement the suggested technique on a device running MATLAB R2014b. The comparison of the results of tumour segmentation and the ground-truth images of brain tumour data sets publicly available are carried out for the evaluation and investigation of the resulting efficacy of the proposed tumour segmentation technique.

Metrics including accuracy, precision, recall, and f-measure are used to evaluate the suggested algorithm's effectiveness. The performance comparison's findings are shown in Table 2. The proposed Modified Graph Neural Network (MGNN) method is compared with the Available-Active Adaptive Neuro Fuzzy Inference System (CANFIS) and Convolutional Neural Network (CNN). The performance metrics based on this confusion matrix are computed as below. The percentage of correctly acquired positive observations and all of the projected positive observations is what determines precision.

$$Precision = TP/(TP + FP) \quad (24)$$

The overall number of properly identified positive observations and the proportion of those that were

Table 2. Performance comparison results.

	Methods		
Metrics	CNN	CANFIS	MGNN
Accuracy	85.11	96.06	98.86
Precision	84.31	91.45	91.69
Recall	81.24	92.12	92.42
F-measure	83.27	91.15	92.05
Error	14.89	3.94	1.13

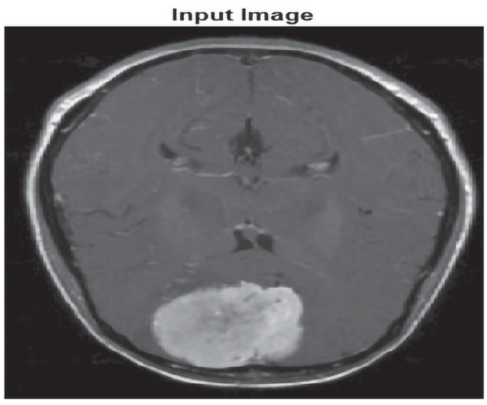

Figure 4. Input image.

observations determine sensitivity or recall.

$$Recall = TP/(TP + FN) \tag{25}$$

F-measure is given by the weighted average of Precision and Recall. Consequently, it uses false positives and false negatives.

$$F - measure = 2 * \frac{Recall * Precision}{Recall + Precision} \tag{26}$$

In terms of positives and negatives, accuracy is calculated as follows:

$$Accuracy = \frac{TP + FP}{TP + TN + FP + FN} \tag{27}$$

where TP – True Positive, FP – False Positive, TN – True Negative, FN – False Negative.

Figure 4 depicts the input brain image, Figure 5 illustrates the Reference Image, Figure 6 demonstrates the results of Image Registration, and Figure 7 Illustrates the clustering results.

Figure 8 shows the results of the accuracy comparison between the suggested MGNN and existing

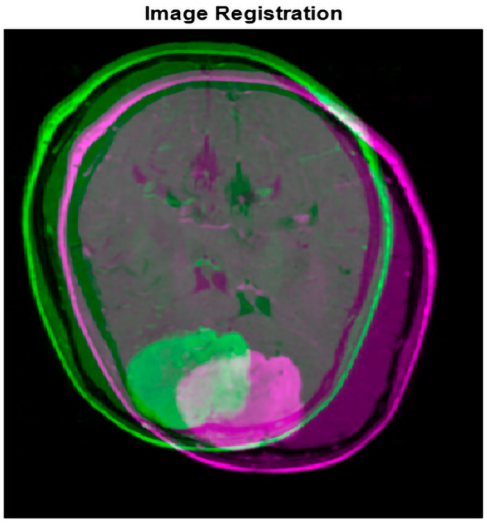

Figure 6. Image registration.

approach for the categorization of the data on ocular illness. The proposed IFCM-based segmentation technique yields the optimal results to improve the classifier accuracy. Overall, the results demonstrate that the proposed machine-learning algorithms do not perform as well for the specific datasets as the MGNN model does, and these results are consistent with the error rate previously discovered and are related to the proposed MGNN classification model's generated rule sets. It can be concluded from the results that the proposed MGNN approach yields the better precision result of 91.69%, whereas the other available CNN and CANFIS techniques yield 84.31% and 91.45%, respectively.

Figure 9 shows the results of recall comparison between the proposed and available techniques used for the brain tumour data classification. The data considered in this research are primarily focused on the diagnosis of individuals showing symptoms of disease

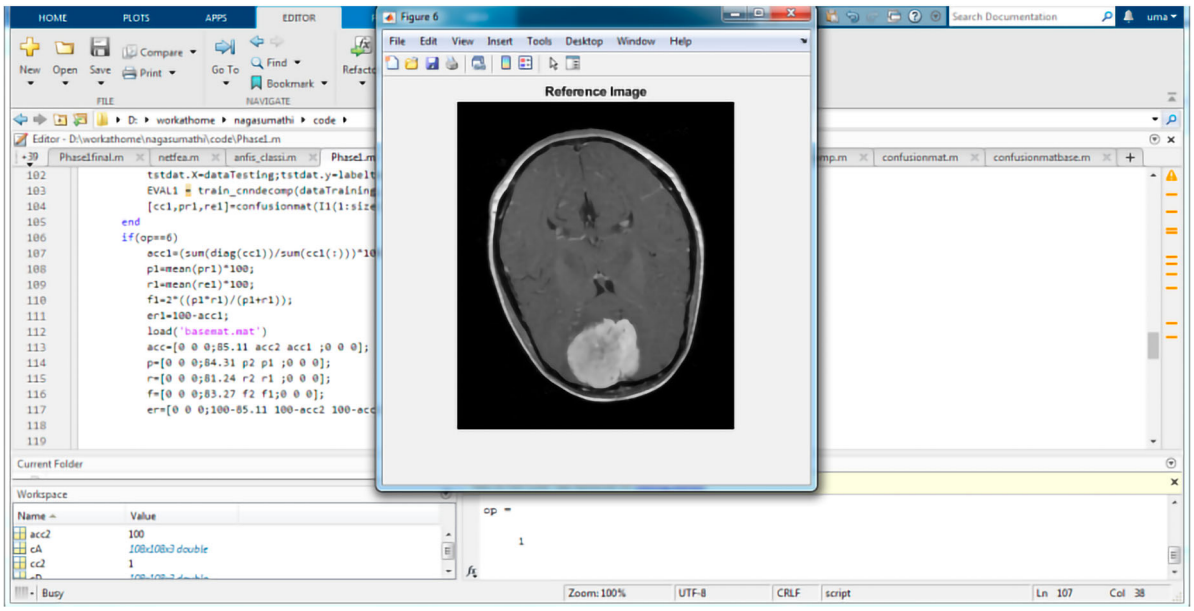

Figure 5. Reference image.

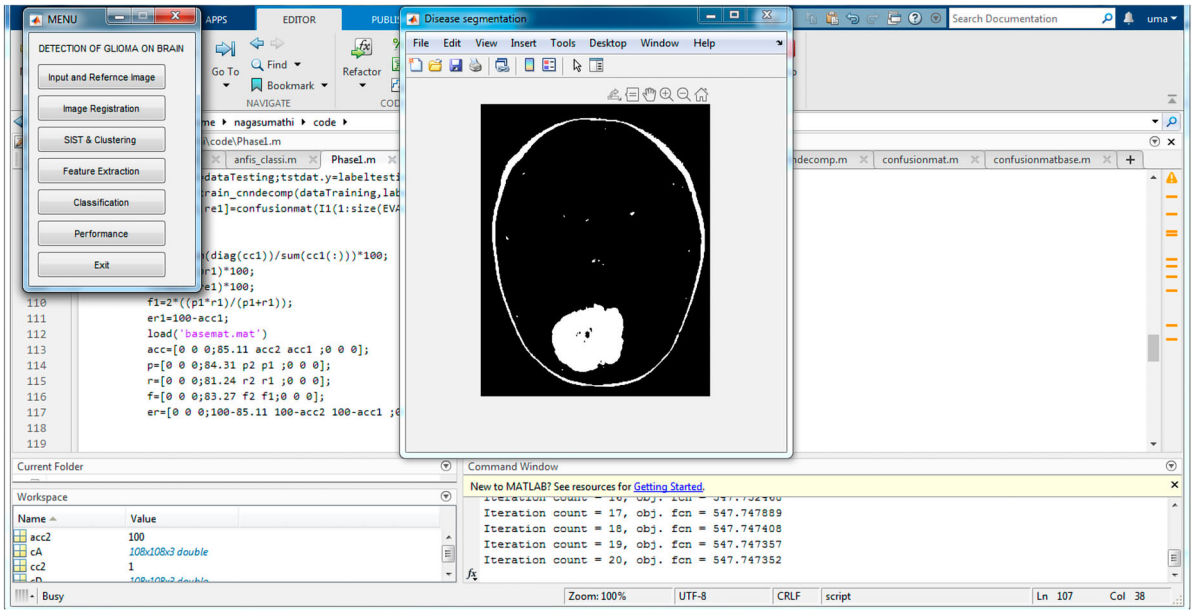

Figure 7. Clustering.

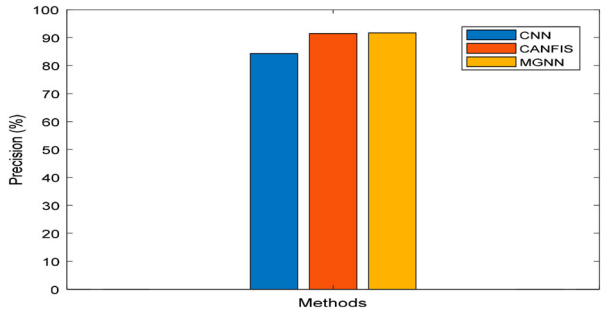

Figure 8. Results of a precise comparison of the proposed and current methods for categorizing data on brain tumours.

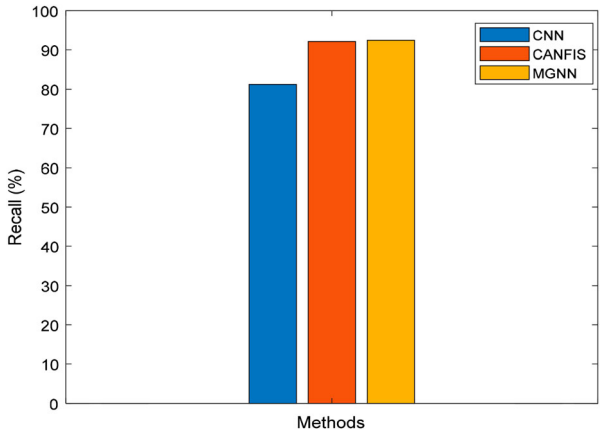

Figure 9. Results of comparing the suggested and current methods for categorizing the data on brain tumours are recalled.

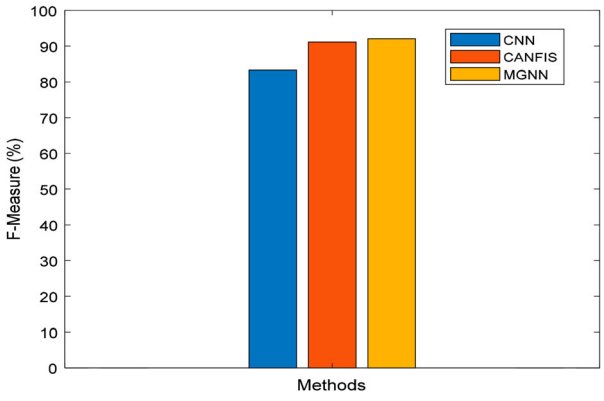

Figure 10. Results of the suggested and current methods for categorizing data on brain tumours using the F-measure.

with different variables generally having an impact on the diagnosing result. The prediction model is thus seen as a classification issue that arises from either having a tumour or not. As a consequence, the suggested MGNN models were employed for the specific job, and the results were then analysed and evaluated. It can be proven from the results that the proposed MGNN approach yields improved recall result of 92.42%, whereas the other available CNN and CANFIS techniques provides 81.24% and 92.12% correspondingly.

Figure 10 shows the results of the *F*-measure comparison between the proposed and available techniques for the brain tumour data classification. Also, a dramatic reduction in the time needed to carry out a prediction during the usage of dimensionality reduction approaches. But, in case the disease is not serious, its classification is difficult. It is found from the above comparison that the proposed model yields the maximum-measure as compared to other deep-learning models, rate measurement in a database. The database considered offers the optimal-measure results in comparison with the other techniques. It can be found from the results that the proposed MGNN approach yields better F-measure result of 92.05%, whereas the other available CNN and CANFIS techniques yield 83.27% and 91.15% correspondingly.

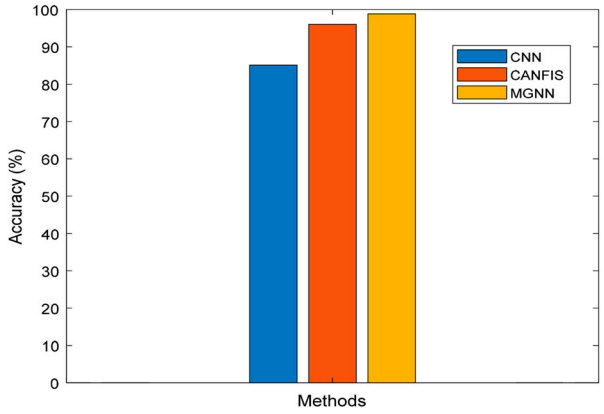

Figure 11. Results of an accuracy comparison of the proposed and current methods for identifying data on brain tumours.

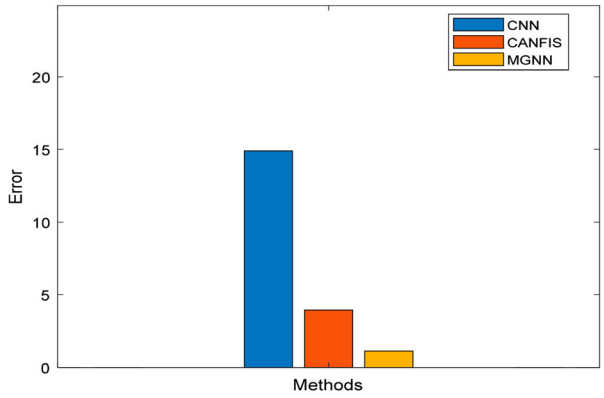

Figure 12. Results of the suggested and current methods for categorizing data on brain tumours in terms of error.

Figure 11 shows the findings of a comparison of the accuracy of approaches for classifying brain tumour data that have been developed and those that are already in use. One who can accurately forecast the target using deep learning is superior and performing the generalization of new instances predictions. Generally, the model is validated in terms of accuracy, which involves two subtypes, which are sensitivity and specificity. It can be proven from the results of simulation that the proposed MGNN model yields improved accuracy of 98.86% while the available CANFIS model provides 96.06% and the CNN model achieves 85.11% correspondingly. It can be proven from the results that the proposed MGNN approach yields better values of accuracy in comparison with the available classification approaches.

Figure 12 demonstrates the results of Error comparison between the proposed and available techniques for the brain tumour data classification. It is found from the results of simulation that the proposed MGNN model yields reduced error of 1.13% while the available CANFIS model achieves 3.94% and the CNN model attains 14.89% correspondingly. It can be proven from the results that the proposed MGNN approach yields reduced error values in comparison with the available classification approaches.

5. Conclusion

In this technical work, a completely automated brain tumour adaptive segmentation and reliable classification model that uses a modified Graph Neural Network (MGNN) is proposed. Image registration, SIST, adaptive segmentation, feature extraction, and tumour classification are the five steps of the proposed module. The training and segmentation of the features pertaining to the modified brain MRI images are performed using IFCM to distinguish between the anomalous brain image and the normal brain image. The experimental findings reveal that the suggested model achieves the maximum accuracy results for breast cancer detection. The Image registration, segmentation with MGNN classification algorithm yields sensitivity of 93.1%, specificity of 98.9%, and 95.67% of accuracy. But, this work focuses on the hybrid in the form of a classification model futuristic approach. In future enhancement, swarm-intelligence based optimization algorithms are used for tune parameters weight and bias to improve classification accuracy.

Disclosure statement

No potential conflict of interest was reported by the author(s).

References

[1] Işın A, Direkoğlu C, Şah M. Review of MRI-based brain tumor image segmentation using deep learning methods. Procedia Comput Sci. 2016;102:317–324. doi:10.1016/j.procs.2016.09.407

[2] Swanson KR, Bridge C, Murray JD, et al. Virtual and real brain tumors: using mathematical modeling to quantify glioma growth and invasion. J Neurol Sci. 2003;216(1):1–10. doi:10.1016/j.jns.2003.06.001

[3] Jalali V, Kaur D. A study of classification and feature extraction techniques for brain tumor detection. Int J Multimed Inf Retr. 2020;9(4):271–290. doi:10.1007/s13735-020-00199-7

[4] Binello E, Germano IM. Targeting glioma stem cells: a novel framework for brain tumors. Cancer Sci. 2011;102(11):1958–1966. doi:10.1111/j.1349-7006.2011.02064.x

[5] Collins VP. Brain tumours: classification and genes. J Neurol Neurosurg Psychiatry. 2004;75(Suppl 2):ii2–ii11.

[6] Sajjad M, Khan S, Muhammad K, et al. Multi-grade brain tumor classification using deep CNN with extensive data augmentation. J Comput Sci. 2019;30:174–182. doi:10.1016/j.jocs.2018.12.003

[7] Trembath D, Miller CR, Perry A. Gray zones in brain tumor classification: evolving concepts. Adv Anat Pathol. 2008;15(5):287–297. doi:10.1097/PAP.0b013e3181836a03

[8] Ayadi W, Charfi I, Elhamzi W, et al. Brain tumor classification based on hybrid approach. Vis Comput. 2020;38(1):1–11.

[9] Chelghoum R, Ikhlef A, Hameurlaine A, et al. Transfer learning using convolutional neural network architectures for brain tumor classification from MRI images.

IFIP International Conference on Artificial Intelligence Applications and Innovations; 2020. pp.189–200.
[10] Selvapandian A, Manivannan K. Fusion based glioma brain tumor detection and segmentation using ANFIS classification. Comput Methods Programs Biomed. 2018;166:33–38. doi:10.1016/j.cmpb.2018.09.006
[11] Mathiyalagan G, Devaraj D. A machine learning classification approach based glioma brain tumor detection. Int J Imaging Syst Technol. 2021;31(3):1424–1436. doi:10.1002/ima.22590
[12] Kibriya H, Amin R, Alshehri AH, et al. A novel and effective brain tumor classification model using deep feature fusion and famous machine learning classifiers. Comput Intell Neurosci. 2022: 1–15. doi:10.1155/2022/7897669
[13] Demir F. Deep autoencoder-based automated brain tumor detection from MRI data. In Artificial Intelligence-Based Brain-Computer Interface; 2022. pp.317–351.
[14] El Hamdaoui H, Benfares A, Boujraf S, et al. High precision brain tumor classification model based on deep transfer learning and stacking concepts. Indones J Electr Eng Comput Sci. 2021;24(1):167–177. doi:10.11591/ijeecs.v24.i1.pp167-177
[15] Naser MA, Deen MJ. Brain tumor segmentation and grading of lower-grade glioma using deep learning in MRI images. Comput Biol Med. 2020;121. doi:10.1016/j.compbiomed.2020.103758
[16] Alnowami M, Taha E, Alsebaeai S, et al. MR image normalization dilemma and the accuracy of brain tumor classification model. J Rad Res Appl Sci. 2022;15(3):33–39. doi:10.1016/j.jrras.2022.05.014
[17] Chuang KS, Tzeng HL, Chen S, et al. Fuzzy c-means clustering with spatial information for image segmentation. Comput Med Imaging Graph. 2006;30(1):9–15. doi:10.1016/j.compmedimag.2005.10.001
[18] Jin W, Ma Y, Liu X, et al. Graph structure learning for robust graph neural networks. Proceedings of the 26th ACM SIGKDD international conference on knowledge discovery & data mining; 2022. pp.66–74.
[19] Poli R, Kennedy J, Blackwell T. Particle swarm optimization. Swarm Intell. 2007;1(1):33–57. doi:10.1007/s11721-007-0002-0
[20] Paulchamy B, Vinothkumar V. Tumor categorization model (TCM) using soft computing techniques for providing efficient medical support in brain tumor treatments. J Med Imaging Health Inform. 2021;01(11):2806–2813.